Available online at www.scientiaresearchlibrary.com

Scientia Research Library

Journal of Applied Chemistry, 2013, 1 (1):23-43

(*http://www.scientiaresearchlibrary.com/arhcive.php*)

Effect of contact temperature rises during sliding on the wear resistance of Al-$FeAl_3$ based Intermetallic composite

Sanjay Srivastava[1]

Department of Materials Science & Metallurgical Engineering
Maulana Azad National Institute of Technology, Bhopal-462051 INDIA

ABSTARCT

In this paper, we have studied the wear and frictional properties of the Al-Fe composite materials. The composite materials with 6.23 and .2 % Fe was prepared by the liquid metallurgical method. XRD and SEM technique were used to study the morphological character of the as-cast composite materials and subsequent forged by pneumatic hammer to homogenize the structure of the material. The optical and SEM results showed homogeneous dispersion of iron particles in the matrix. A dry sliding wear tests of as cast and forged samples was conducted on pin-on-disc machine over wide ranges of applied load and sliding speed. To determine the wear mechanisms, the worn surfaces of the samples were examined by SEM. Debris and wear tracks have been studied in detail to analyze the surface effects during dry sliding and to correlate wear properties. Observations from the experiments showed that the wear mechanism is dominated by oxidative debris under low loads and sliding velocities and wear tracks were largely covered with a smooth oxide layer.

Keywords: Al-Fe composite, Liquid metallurgy, Wear rates, Coefficient of friction, Worn surface,

---

INTRODUCTION

Superior mechanical properties can be obtained when fine and stable reinforcements with good interface bonding are dispersed uniformly in the matrix. The matrix may be metal, ceramic or polymer. In conventionally produced particulate-reinforced metal matrix composites (MMCs), the size of reinforcement particles are larger than that of dispersed phase and the particles are located at the inter granular position of metal matrix. The mechanical properties of MMCs are controlled by the size and volume fraction of the reinforcements as well as the nature of the matrix-reinforcement interface [1].

The MMCs have unified combination of metallic properties of the matrix with the ceramic properties of the reinforcement, such as high specific modulus, high specific strength, and thermal stability. Thus they have the potential to serve a wide spectrum of applications in aerospace, automotive, electronic, and recreation industries. The focus has increasingly shifted toward discontinuously-reinforced composites as a competition for continuous fiber reinforced composites from the standpoint of isotropic mechanical properties [2-8].

Metal-matrix composites show a combination of superior mechanical properties, such as a better elastic modulus, tensile strength, and high-temperature stability in comparison with an unreinforced matrix, yet they suffer from poor tensile ductility, fatigue-crack growth resistance and fracture toughness. The sliding wear of the composites is a complex process involving not only mechanical but also thermal and chemical interactions between the surfaces in contact. Particle-reinforced metal-matrix composites are recognized as having a better wear resistance due to the presence of hard particles.

These materials can be used as a reinforced part in pistons and in several wear-resistant applications. The aluminium alloys are reported to have an increase in wear rate as change the sliding speed and load. In general, several factors affect the wear equations, such as operational parameters, topography of the surface contact, geometry, speed, load, and coefficient of sliding friction. In addition, material and environmental parameters, various material hardness, temperature, elasticity, breakage, as well as thermal properties, also affect wear. The degree of wear is the result of several common factors applied in certain cases, particularly the relationship between the rate of corrosion and load, speed, coefficient of friction, and adhesion, as well as hardness and tensile strength of the material. Chow et al., [9] reported the effect of normal load and sliding speed of friction and wear on the property of an aluminum disk against stainless steel pin. Results showed that the value of the coefficient of friction increased with increasing sliding speed in normal for aluminum. Ramachandra et al., [10] reported that wear increased with increase in normal load and sliding velocity. Hardness increases with a continuous or intermittent increase in SiC particles and is related to friction and adhesion. Abbas and Ibrahim [11] studied the effect of Cu and Mg adds on wear behavior of (Al-8% Si) under dry sliding conditions and they concluded that the hardness and wear resistance increase because of formations of hard second-phase particles such as Al2Cu (θ) and CuMgAl. The reinforcement phase is generally one of the following: continuous boron or graphite fibres, or hard particles such as SiC and A&O, in discontinuous particulate or whisker morphology. The phenomenon of increase in wear rate at longer sliding distances and increase in the applied load was also reported [11-13]. Nickel aluminide-based intermetallic compounds have low density, good oxidation resistance and metal-like properties, which makes them attractive materials for a wide range of applications.

Iron aluminides based on DO_3 or B_2 ordered structure are now showing extensive attention as materials with good potential for industrial applications such as replacements for high temperature oxidation-resisting or corrosion-resisting stainless steel. The Fe-Al equilibrium phase diagram is shown in **Fig 1,** the intermetallic phases with allowable mechanical properties in case of weldings' is marked. The system is characterized with an iron-based solid solution and six non-stoichiometric intermetallic compounds of Fe_3Al, FeAl (D_2), $FeAl_2$, Fe_2Al_3(H), Fe_2Al_5 and $FeAl_3$. **Table 1** indicates crystal structure, range, stability and hardness for this phase diagram with special emphasis on the IMPs [14]. These materials have a lower density and hence they offer a better strength-to-weight ratio when it's compared with the stainless steels. The wear resistance of Al3Fe alloy was found to vary with ductility and yield strength. Most of the $FeAl_3$ grains contain a large amount of microtwin presumably due to high stress caused by the volume expansion associated with the formation of the Fe_3Al phase. FeAl presents a B2 (cP2) crystal lattice, which comes from the body-centered cubic structure. The unit cell contains 8 aluminum atoms, 1 in each corner, which are shared with the other 8 unit cells surrounding the 1 aluminum atom, which is typical for the BCC structure. As the cP2 structure can be seen as 2 interpenetrating primitive cubic cells, the iron or nickel atoms are supposed to occupy the corner of the second sublattice.

Bouche´et al., [15] were reported by a melt bath technique by Fe/Al diffusion couples, and then isothermally annealed at temperatures of 973–1173 K. A similar experiment was conducted by Bouayad et al [16]. In the binary Fe–Al system,1) $FeAl_3$, Fe_2Al_5, $FeAl_2$ and FeAl are the stable

compounds at these temperatures. According to their experimental results, however, only Fe_2Al_5 and $FeAl_3$ are formed as visible layers at the Fe/Al interface in the diffusion couple owing to annealing. The thickness is much smaller for the $FeAl_3$ layer than for theFe_2Al_5 layer, and irregular tongue-like morphology is realized for the Fe_2Al_5 layer. Such formation behavior of Fe_2Al_5 and $FeAl_3$ was reported also in the other studies.

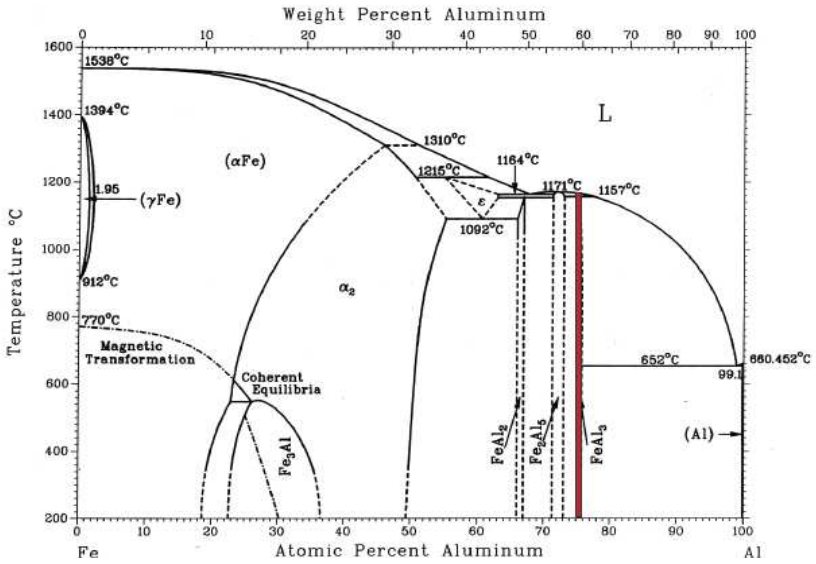

Figure 1: Fe-Al equilibrium phase diagram [5]

Table 1: Crystal structure, stability range and hardness of the phases formed in Fe-Al binary System at room temperature [13,14]

Phases	**Crystal structure**	**Stability range (at.%)**	**Vickers Hardness (9.8N)**
Fe solid solution	BCC	0-45	Not investigated
γ-Fe	FCC	0-1.3	Not investigated
FeAl	BCC (Order)	23-55	470](491 – 667)]
Fe_3Al	DO3	23-34	330 (344 – 368)
Fe_2Al_3	Cubic (complex)	58-65	Not investigated
$FeAl_2$	Triclinic	66-66.9	Unknown (1058 – 1070)
Fe_2Al_5	Orthorhombic	70-73	1013 (1000 – 1158)

$FeAl_3$	Monoclinic	74.5-76.5	892 (772 – 1017)
Al solid solution	FCC	99.998-100	Not investigated

Although there are several techniques for processing of composite materials, large scale production includes the liquid metallurgical (LM) or powder metallurgical (PM) routes. In the former, the particulate phases are mechanically disperse in the liquid before solidification of the melt. However in the latter, either elemental or pre-alloyed powders are blended with particulates and compacted by hot pressing and hot extrusion processes. Forging and heat treatment of the conventional aluminum-alloys improve dimensional stability [9] and ductility [10-12]. In general, the heat treatments lead to a reduction in hardness and tensile strength [13, 11, and 14] of the materials.
This research paper is to investigate the effect of forging on the hardness, wear behavior, and friction of the Al-Fe composites reinforced with variable percentages of iron, produced by the liquid metallurgical technique.

MATERIALS AND METHODS

Selection of materials and Preparation of alloys

Commercially pure aluminum (99.8%), electrolytic iron powder of 50 μm size samples was used for the preparation of Al-Fe composites with different compositions. The experimental setup used for mixing and casting of composites is shown in Fig 2. It is comprised of a cylindrical Sillimanite crucible of 150 mm diameter and 250 mm depth with attachment of four baffles to its sidewalls for proper dispersion of the second phase in melt during stirring. The crucible was placed in an electrically heated muffle furnace. It was also equipped with a bottom pouring attachment, which could be closed or opened by a graphite stopper with a lever system. A steel mold was placed beneath the furnace to cast the molten metal. In the top cover an opening was provided to charge materials and for fixing of thermocouples. The temperature of the furnace could be controlled with an accuracy of about $\pm 5^{o}$C. The metallic bath temperature was measured continuously by chromel/alumel thermocouple. The agitator system could be raised or lowered with the help of the hanger and steel frame structure. After adjusting the mixer in a "l" position, the motor was bolted and locked. Three-blade impeller was used for effective mixing. This design provides a very high rate of shear and only axial and radial flow currents are utilized for mixing without any significant vortex formation due to the presence of baffles. The Al-Fe composites were prepared using **the liquid** metallurgical route. The required amount of aluminum (commercial pure grade) was charged into the crucible and aluminum was heated to a temperature above its melting point $200\ ^{0}$ C i.e. 862 ^{o} C. A mechanical stirrer was used for agitation of the melt, at a speed of 2100 rpm. Subsequent iron powder (50-μm-size electrolytic grade) was charged into the melt and the stirring continued. The addition of iron particulate into the melt was facilitated by the vortex created by stirring action and the mixing was carried out for 60 seconds. The emulsion was poured into a chilled cylindrical mold placed beneath the crucible. The procedure was repeated with different compositions. The cylindrical casting of length 20 cm and dia. 2 cm was obtained.

Evaluation of as-cast Properties of the Composite

The wet chemical analysis was used to determine the percentage of iron in the bulk materials and the EDAX analyses was also carried out for confirmation. The microstructure and morphological characteristics of the specimen were studied using optical microscopy and SEM respectively. The presences of iron at the grain boundaries and inside the grain were studied using EPMA. X-ray diffraction analysis was carried out to find the phase present. The densities of the composite were determined using the Archimedes principle by weighing in water and air.

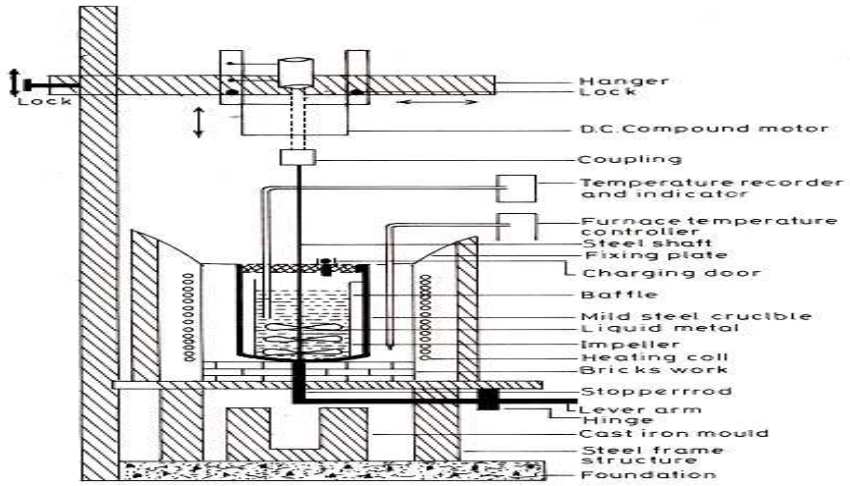

Fig: 2-Schematic diagram of casting set-up

Physical and mechanical tests

In determining the hardness of the composite of Al-Fe, Vickers hardness testing machine was used. The applied load during the testing was kept to be 5 kgN with a dwell time of 20 seconds. Four indentations were made at random locations for all the samples. Two indentations were performed on the top face and two on the bottom and the average values of the lengths of the diagonals of the impressions were used to calculate the Vickers hardness number. The tensile strength and percentage elongation of the alloys were measured using round specimens with a diameter of 8mm and a gauge length of 40mm at a strain rate of 5.9×10^{-3} s^{-1}. All these physical parameter and mechanical properties were determined by taking the average of at least three readings. **.** The stress developed in the composite along with percentage elongation and reductions in the area were computed from the results.

Forging and annealing procedure

Table 2 shows the selected parameters for forging. The forging experiments were carried out for two compositions using pneumatic hammer under constant load. For the forging operation, cylindrical samples of dimension of 60 mm x 25 mm were prepared. These were homogenized at 450 ^{o} C for 20 hours. Before forging composites were soaked for 1.5 hours at 510 ^{o} C. After homogenization and soaking, the composite samples were subjected to 50% reduction in perpendicular, using pneumatic hammer and were quenched immediately in water.

Wear test

Pin-on-disc machine was used for evaluating the wear properties under dry sliding condition. The cylindrical test pin of 8 mm in diameter and 40 mm in length was used against a hardened steel disc 120 mm diameter. In this test the flat end of Cylindrical specimen 8 mm in diameter and 12 mm length was fixed in chuck jaws to prevent specimens from rotating during the test. Axial load was applied to the pins against the plane surface of the rotating disc.

Table 2- Selected parameter of the forging operation

S. No.	***Operation***	***Parameter***
1	***Dimension***	60x25mm
2.	Homogenization temperature	450^{o}
3.	Homogenization time	20hrs
4.	Operation	Forging
5.	Soaking temperature	510^{o}C
6.	Soaking time	1.5 hours
6.	Direction	Perpendicular to diameter
7.	Reduction	50%
8.	Quenching media	Water

Each specimen was weighed before the experiment and after it with a digital balance having sensitivity of 0.001 mg. The duration of the experiment was controlled by a digital timer. The average value of the weight loss percentage as a function of test time was calculated. From weight loss of the specimens (Δm) it is possible to evaluate a dimension less parameter known as , "wear rate" [**17**]. Wear testing was conducted at varying sliding distance, load and sliding velocity. Wear debris was analyzed by X-ray diffraction analysis.

$$W = \frac{\Delta m}{\rho v t A}$$

Where Δm = weight loss (g) ρ= average density of material t = test time (s) A = apparent contact area (mm^2)

RESULT AND DISSCUSION

Result evaluation of as cast Structure

Chemical Analysis

Conventional Method

The wet chemical analysis was used to determine the percentage of iron in the composites. Volumetric method is one of the most versatile techniques for the determination of the element present at the microscopic level. In Al-Fe composites, iron is the minor constituent phase thus the volumetric titration a method is used for analysis. Specimens from different sections were analyzed to find out the uniformity of dispersion and the results are tabulated in Table 3.

EDAX Analysis

Further to confirming the presence of iron in the composites, energy depressive X-ray analysis (EDAX) was also used. Figs 3 and 4 show the EDAX monographs of the composite with two different compositions. In these monographs, the larger peaks correspond to aluminum and smaller ones to iron. It confirms the presence of iron in the Al-Fe composites. The result obtained by EPMA analysis is in agreement with that of EDAX.

Table 3-Chemical composition of Al-Fe composites

Composite	wt.% Fe	wt.% Al	Theoretical density	Experimental Density
Al-6.23%Fe	**6.23**	**-do-**	**2.96**	**2.79**
Al-11.2%Fe	**11.2**	**-do-**	**3.28**	**3.08**

3.2 Physical analysis

Density Measurements

Table 3 shows the physical properties of the different Al-Fe composites. It is observed from the table that density increases from 2.79 to 3.08 with increasing iron content.

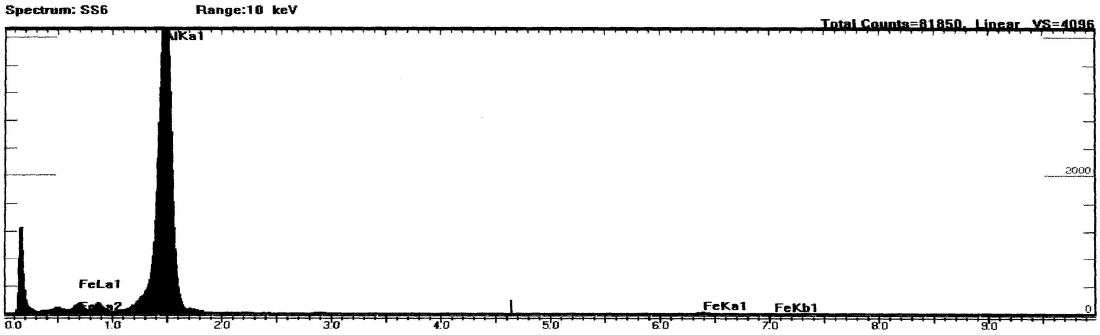

Fig.3-EDAX monograph of Al-6.23%Fe composite

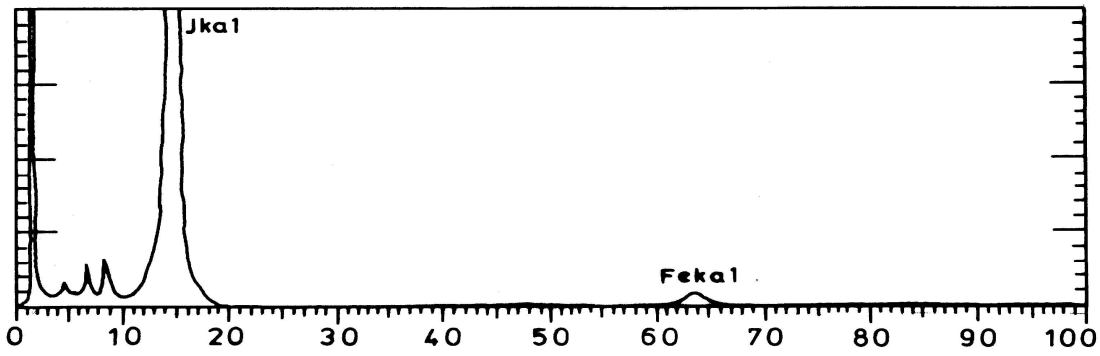

Fig.4-EDAX monograph of Al-11.2%Fe composite

Analysis of Mechanical Properties

The mechanical properties of the composites are tabulated in Table 4. As shown in the table 3, the ultimate tensile strength increases from 142 to 184 MPa and 0.2% off-tensile stress increases from 59 to 83 MPa as the iron increases in the composites from 6.23 to 11.2 wt %. Thus the addition of iron shows a strengthening effect. However percentage elongation decreases from 32 to 17 as the iron content increase. Table 3 also shows the hardness values for all the four composites with different compositions and treated processing. Hardness of the composites increases from 95 to 179 HV with increase of iron. The mechanical properties of cast aluminum/alloys are adversely affected by the presence of iron as large primary or pseudo-primary crystals [**13, 14]**.

Table 4- Mechanical properties of the Al-Fe composite

S.No.	Composite	VHN	UTS(MPa)	0.2%PS(MPa)	% elongation
1	**Al-6.23%Fe**	**163**	**159**	**74**	**27**
2	**Al-11.2%Fe**	**179**	**184**	**83**	**17**

Metallographic analysis

Figure 5 and 6 shows the optical micrographs of composites with 6.23 and 11.20 % Fe at different magnifications. These figures clearly reveal the presence of larger amounts of second phase particles. These second phase particles exist in the elongated form. These elongated forms appear in the needle shape at higher magnification. The needle shaped intermetallics is found to be increasing with iron content. All the composites were also studied using SEM to find out the morphological features in details. Figure 7 and 8 shows the SEM micrographs of all the composites used for the study. At the lower magnifications, clusters of Al-Fe intermetallics are seen, and the needle shaped intermetallics were clearly visible at the higher magnification. XRD analysis was conducted for all the four samples produced with different iron percentages in the matrix. XRD patterns for different compositions are shown in Figure 7c and 8c. In these curves large peaks corresponds to the major phase aluminum and the smaller one corresponds to $FeAl_3$ [19, 20].

Result evaluation of Forged sample

A.Structural properties

The structural characteristic of the specimen after forging was studied using optical microscope and scanning electron microscope. Figures 9 a and b show the optical micrographs of the forged Al-Fe specimens with 6.23 and 11.2% iron. Fig. 5-8(a-b) in as-cast conditions show the fine network of needle shaped intermetallics of $FeAl_3$. However after forging, intermettalics transform to rhombohedral shape as shown in Figure 9 a and b. To further clarify the structure, the Al-Fe specimens with 11.2 % iron as also studied under SEM, and the results are shown in Figure 10 a and b. These results confirmed the presence of intermettalics in the rhombohedral shape.

A. B.

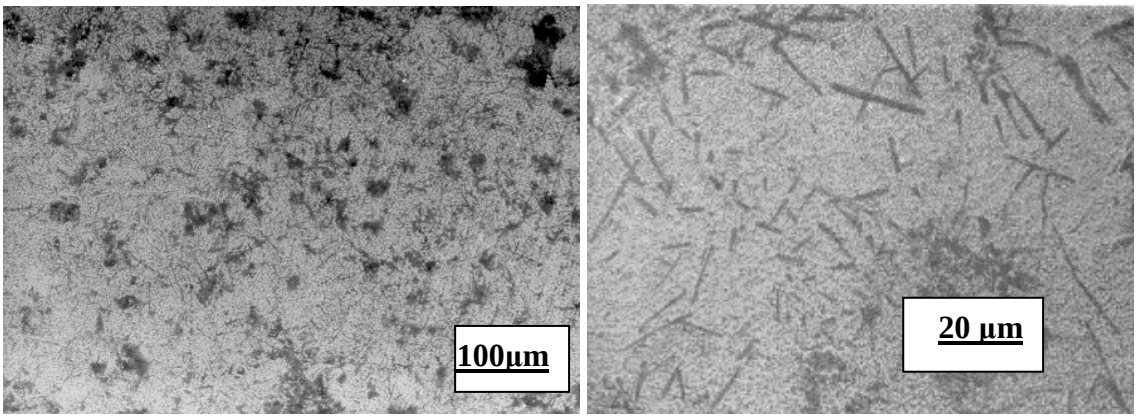

Fig 5-Optical micrographs of Al-6.23% Fe composite at different magnifications (a,b)

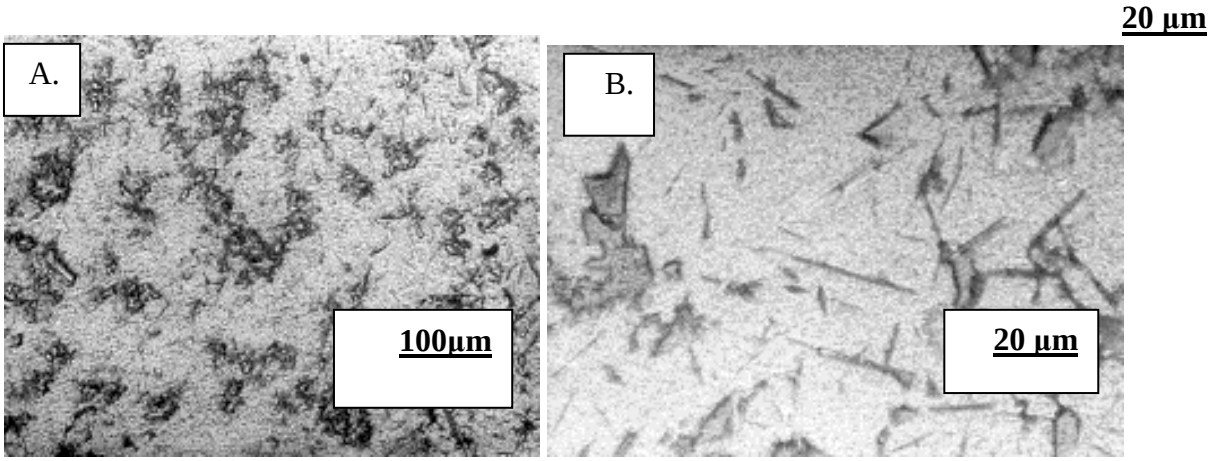

Fig 6-Optical micrographs of Al-11.2% Fe composite at different magnifications (a, b)

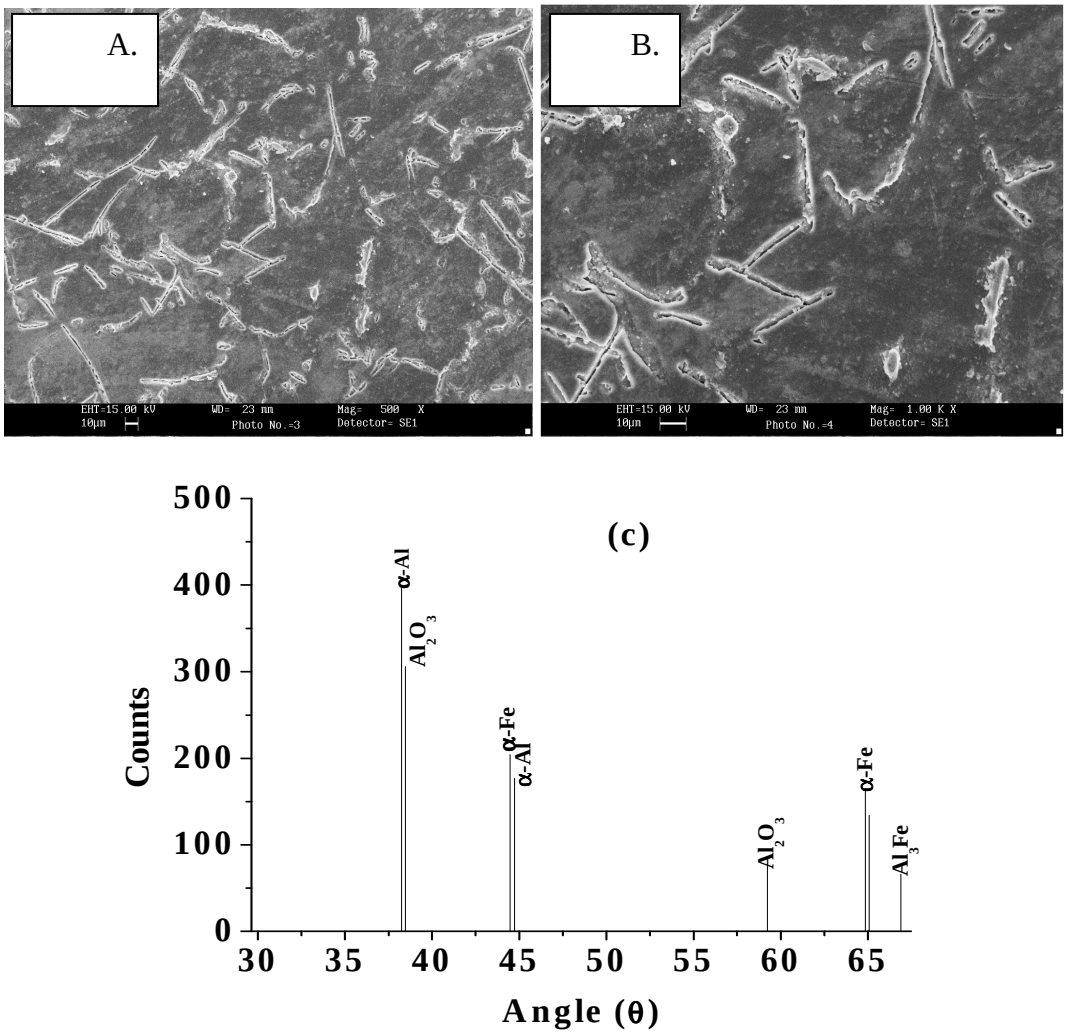

Fig.7-SEM micrographs of Al-6.23% Fe composite at different magnification (a,b) and (c)XRD graph showing presence of $FeAl_3$.

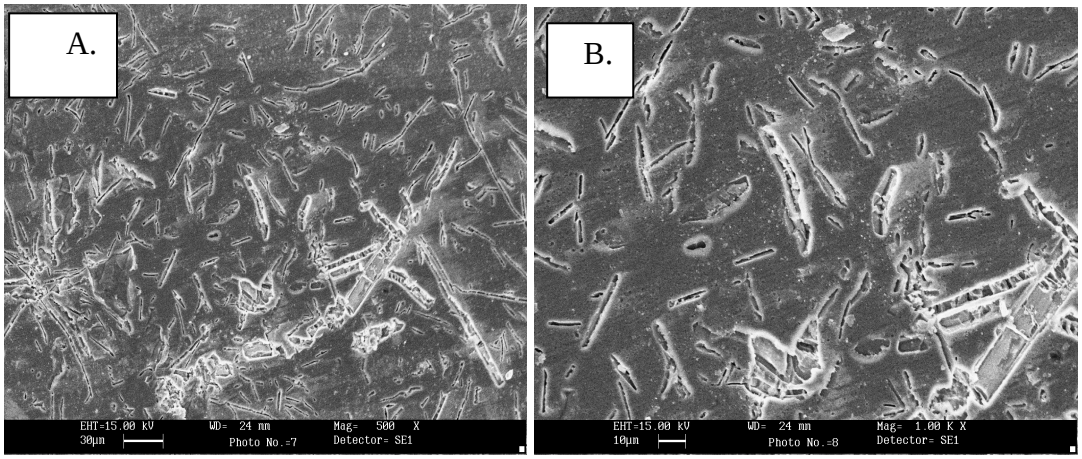

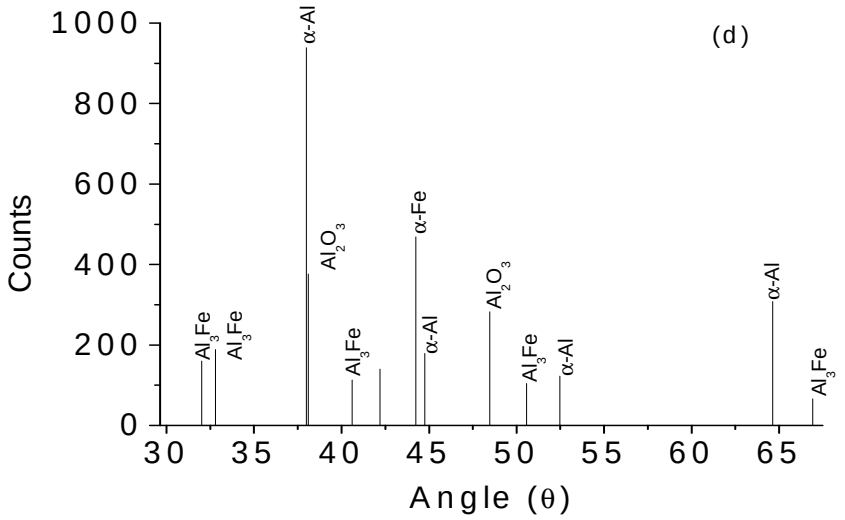

Fig.8- SEM micrographs of Al-11.2% Fe composite at different magnification (a,b) and (c)XRD graph showing presence of $FeAl_3$

B.Mechanical Properties

The mechanical properties of forged composites along with as-cast composite are tabulated in Tables 4. The results show improved mechanical properties of forged samples in comparison with as cast composites. The UTS, proof stress and hardness increases and ductility decrease after forging. This can be attributed to the formation of $FeAl_3$ intermetallic by transformation. Due to forging, the internal stresses are also generated within the materials. This internal stress modifies the properties of the composite materials. In all the cases the higher percentage of the iron results in improved mechanical properties.

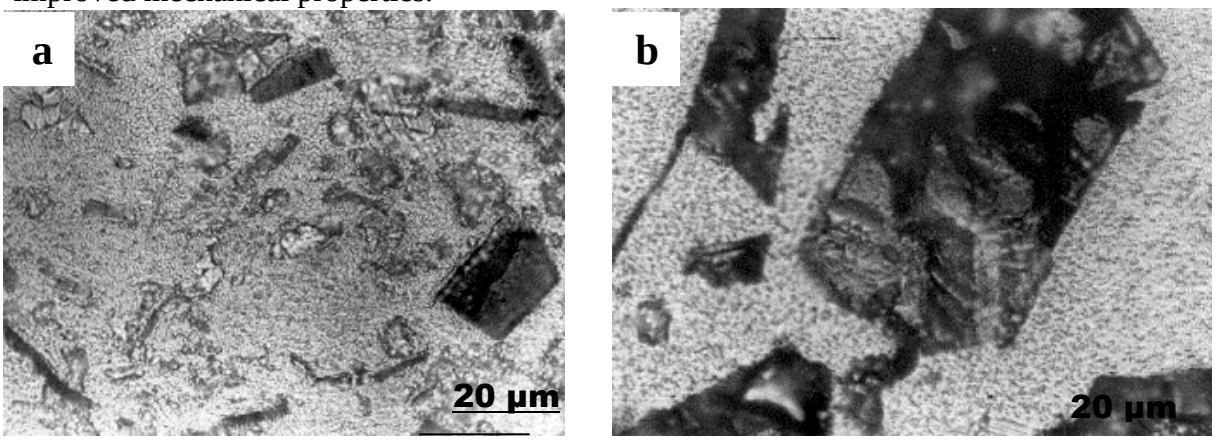

Fig. 9- Forged microstructures of Al-Fe composites with different iron percentage (a) 6.23% and (b) 11.2%

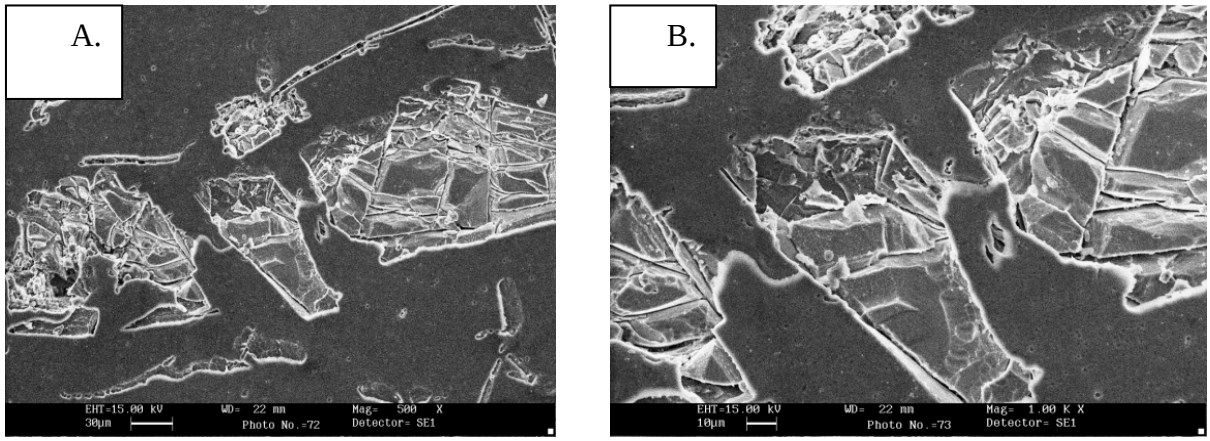

Figs.10- SEM micrographs of Al-11.2%Fe composites showing the presence of rhombohedral intermettalics at different magnifications.

Table 4- Mechanical Properties of Al-Fe composites

S.No.	Property Measured	As Cast Sample		Forged sample	
		Al-6.23%Fe	Al-11.2%Fe	Al-6.23%Fe	Al-11.2%Fe
1.	Hardness	163	179	197	217
2.	UTS, MPa	159	184	220	260
3.	0.2% Proof stress, MPa	74	83	99	127
4.	% elongation	27	17	11	5

C. Wear studies

Figure 11 shows the variation of bulk wears along with rise of temperature during the investigation with sliding distance at 3kg load and 0.772 m/s sliding velocity. It is observed that the initial running-in period is followed by the steady state wear for all the composites. In steady state wear, it shows a linear relationship between the wear volume and sliding distance. The bulk wear decreased with increasing in iron content. Almost a linear relationship is observed in bulk wear and sliding distance i.e. steady state wear is observed after initial running-in period of 500-1000m in almost all the case irrespective of load or sliding velocity used. The forged Al-11.2% Fe sample shows lowest bulk wear among all the composite which may be due to that high amount of hard phase formed, increase the overall hardness of the composite material. It is also evident from the Figure 11 that to increase the sliding distance, the test specimen attends the equilibrium temperature due to rubbing. The relation found here is in accordance with the pattern for most metallic materials derived theoretically as well as observed experimentally. However, at a higher combination of load and sliding velocity, the wear volume is higher for all the four composites.

The studies conducted, to see the effect of applied load on wear rate, reveal that wear rate increases continuously with load in a linear manner, as it is evident from Figure 12 at a particular velocity. Figure 12 shows the variation of temperature of the test sample vs loads. At the higher loads, the

maximum heat is generated within the sample. It can be seen from the Figure 13, that the as cast-Al-11.2%Fe composite shows the minor rise in temperature than the as cast Al-6.23 % Fe composite while the reverse situation is found in the forged composite. The forged Al-11.2% Fe composite has a maximum capacity to dissipate the friction heat. Therefore the melting of the sample surface during the experiment is less possible in the forged Al-11. 2%Fe composites as compared to forged Al-6.23 % Fe composite.

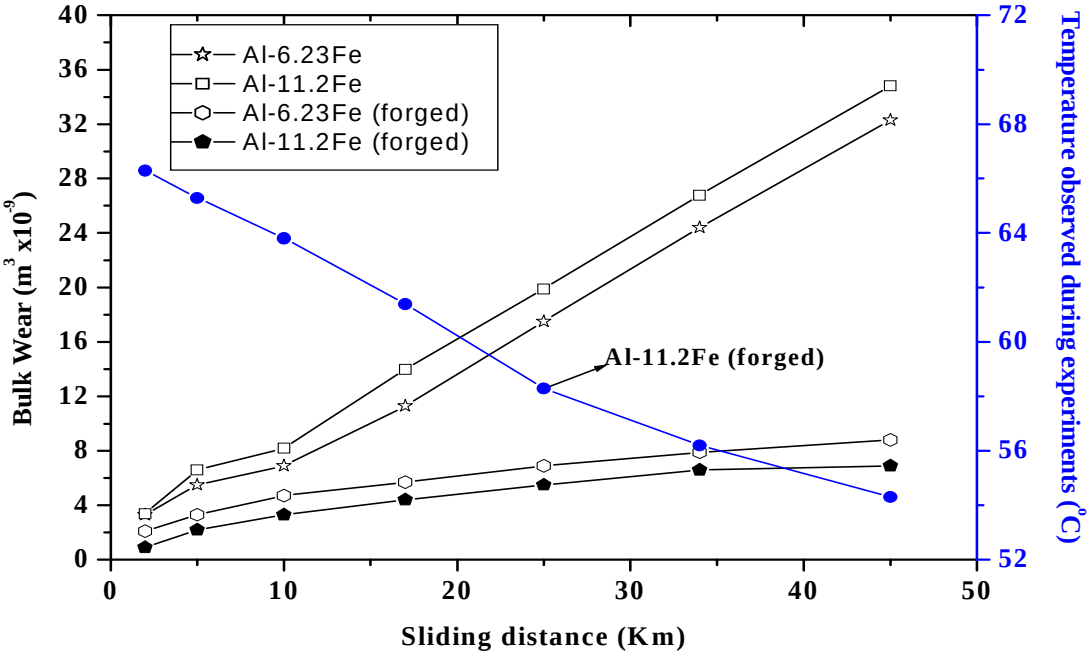

Fig.11 Variation of bulk wears with sliding distance at 3 kg load and 0.772 m/s sliding velocity for as-cast Al-Fe composites (a) Al-11.2 %Fe (d) Al-6.23%Fe (a) Al-6.23%Fe(F) (b) Al 11.2%Fe (F).

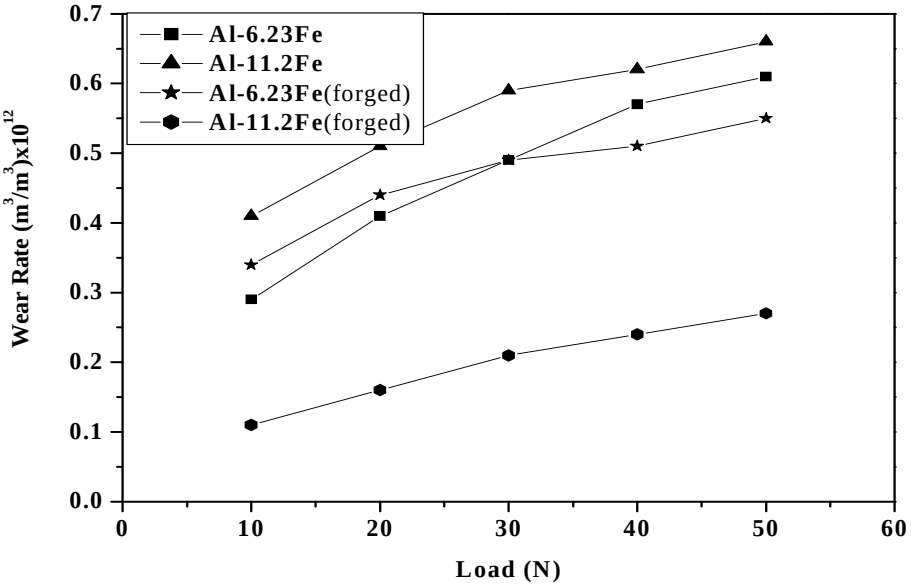

Fig 12. Variation of wear rate with a load at 2.3549 m/s sliding velocity for as-cast Al–Fe composites (a) Al-11.2 %Fe (d) Al-6.23%Fe (a) Al-6.23%Fe(F) (b) Al 11.2%Fe (F)

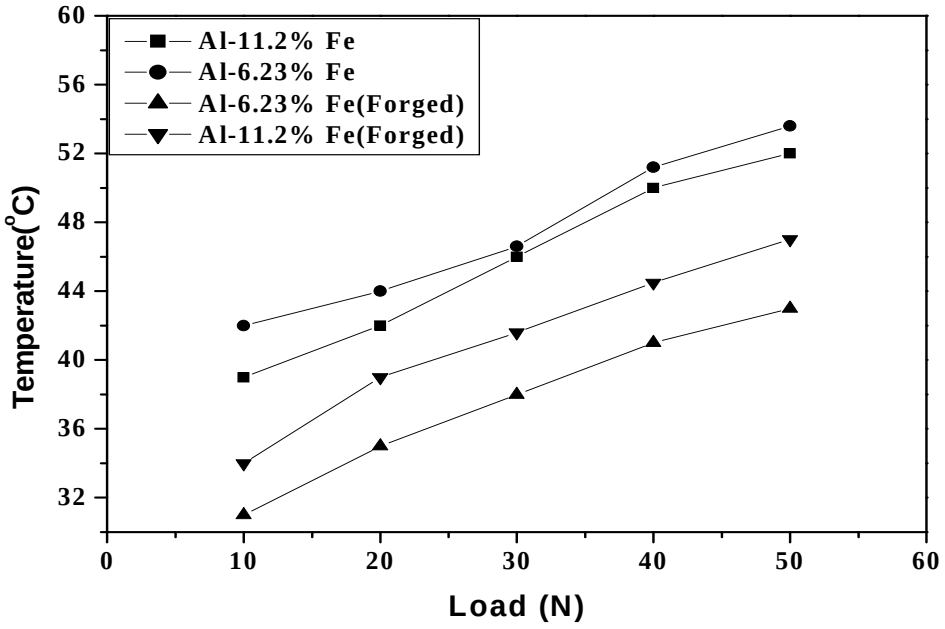

Fig 13. Variation of Temperature with a load at 2.3549 m/s sliding velocity for Al–Fe composites. composites (a) Al-11.2 %Fe (d) Al-6.23%Fe (c) Al-6.23%Fe(F) (d) Al 11.2%Fe (F)

Figure 14 shows the variation of wear rate with sliding velocity at 1-kg load. Like other aluminum alloys/composites, all the Al-Fe composites show an initial decrease in wear rate

followed by a sharp increase in wear rate after attaining minima on the worn surface at different loads. Figure 15 shows the variation of temperature of friction surface with sliding velocity. In all the case, the temperature increases linearly with sliding velocity. Similarly the forged, Al-11.2%Fe composite shows the minimum raise in temperature during the test experiment. It is also evident that the forged Al-11.2% Fe composite has maximum hardness, so it has also capacity to sustain a load or bear maximum velocity. The heat dissipation rate of the composite is high. Therefore these materials can also be used at the high velocity without any deformation in the materials.

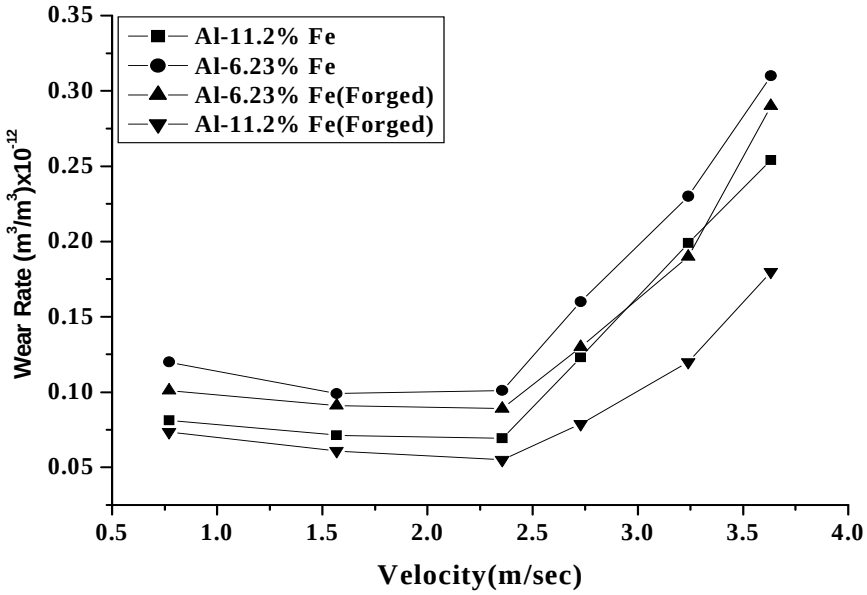

Fig.14- Variation of wear rate with sliding velocity at 1 kg load for Al–Fe composites (a) Al-11.2 %Fe (d) Al-6.23%Fe (c) Al-6.23%Fe(F) (d) Al 11.2%Fe (F)

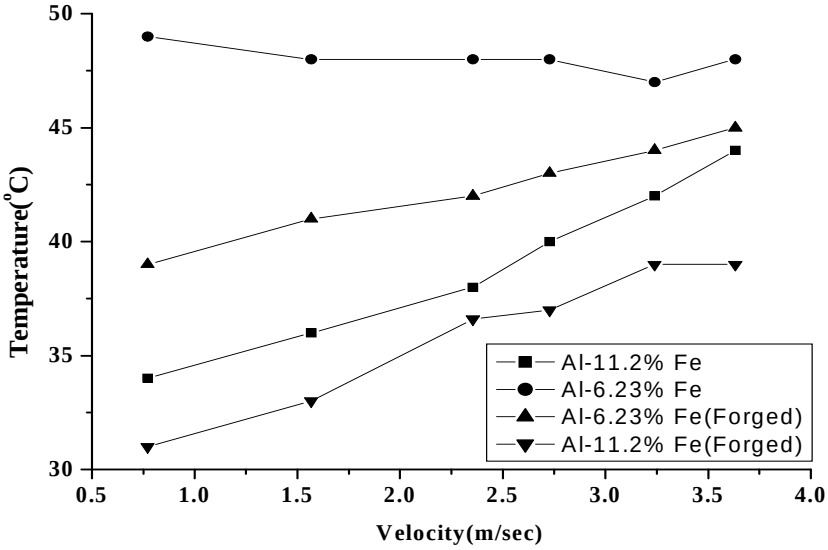

Fig15. Variation of temperature with sliding velocity at 1 kg load of Al–Fe composite (a) Al-11.2 %Fe (d) Al-6.23%Fe (c) Al-6.23%Fe (F) (d) Al 11.2%Fe (F)

Figure 16 and 17 shows the SEM image study of the wear track of the cast and forged Al-11.2 % Fe composite at a different sliding distance. Wear debris is also examined with SEM. Debris of the cast Al-Fe composite at a sliding distance of about 1430 m shows mainly oxidative nature and wear track is smooth with thin oxide layer as shown in Figure 16 a, whereas at a distance of about 40000 m debris comprises different oxides with metallic particle and wear track is observed with a thick oxide layer with deeper track as shown in Figure 16 b.

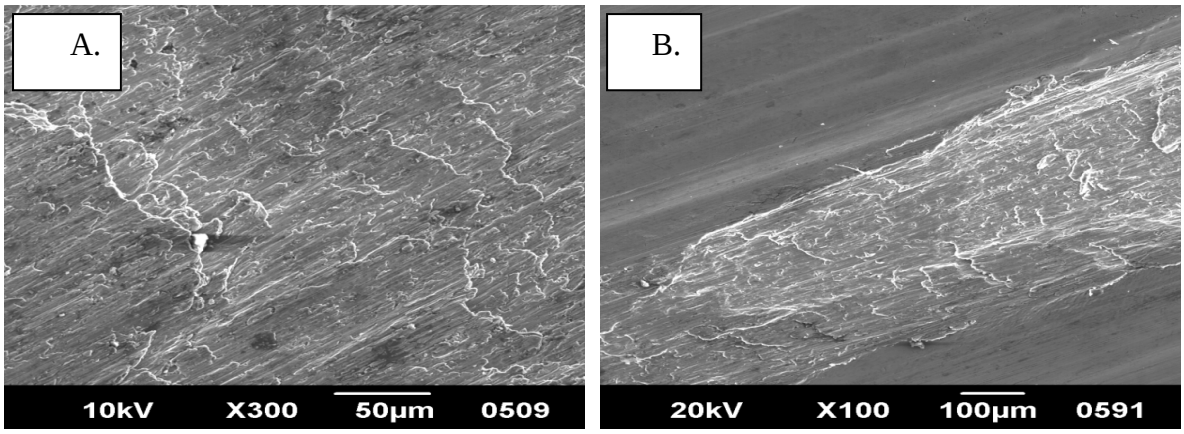

Fig 16. SEM micrographs of wear tracks of Al-11.2 wt.% Fe composite for 1 kg applied load and 2.3549 m/s sliding velocity at different sliding distances of (a) 1429 m and (b) 40009 m.

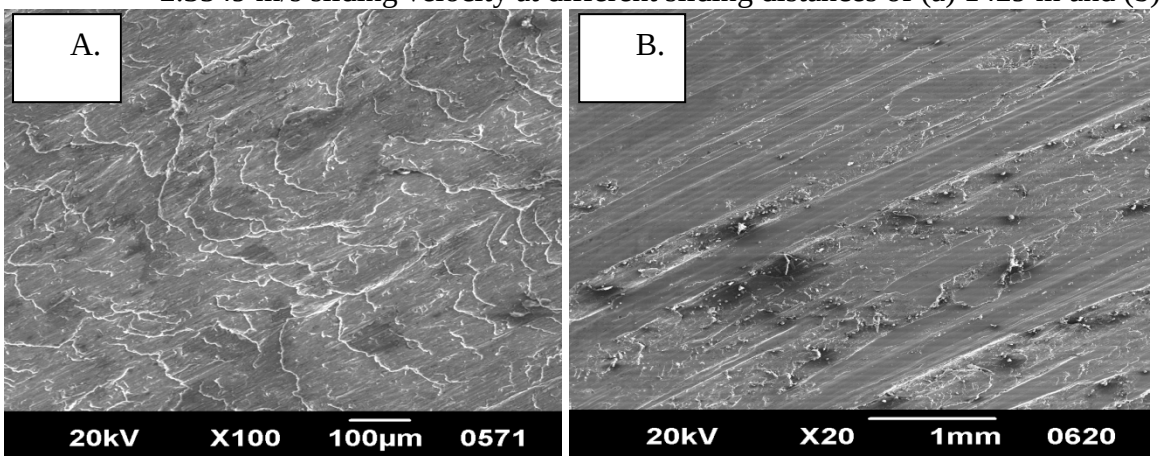

Fig 17. SEM micrographs of wear tracks of Al-11.2 wt.% Fe composite for 1 kg applied load and 0.772 m/s sliding velocity at different sliding distances of (a) 1429 m and (b) 40009 m.

The mechanistic approach is varied with change of velocity and load. Due to examination of wear track and debris as show in Figure 17 & 18 a and b, the oxidative -metallic to metallic wear is observed as applied load and sliding velocity. The adherence of the oxide film at the surface of the bulk material depends upon the processing condition. Out of the several parameters, velocity and load are the important which remove the layer from the surface. The oxide film is broken at the higher velocity and load and deep groove and delamination of surface is observed as shown in Figure 18.

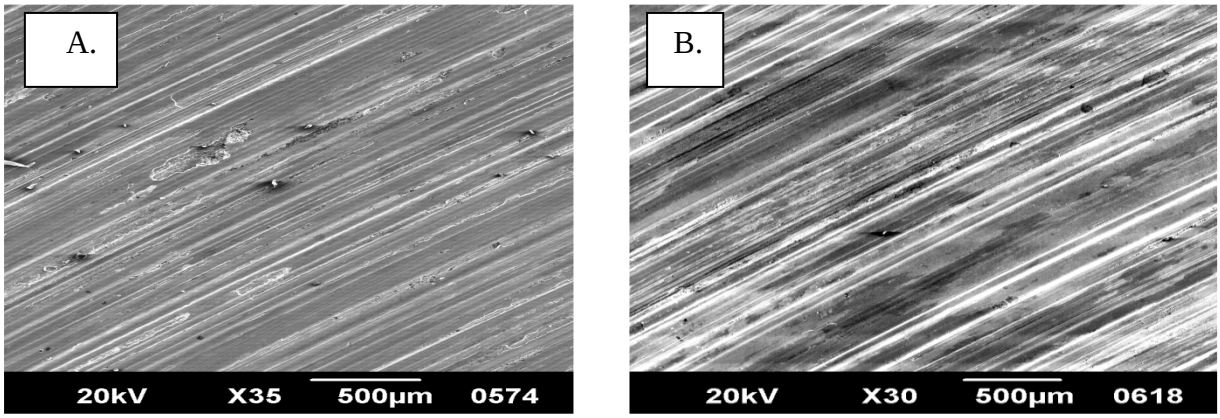

Fig 18. SEM micrographs of wear tracks of Al– Fe composite for 0.772 m/s sliding velocity and at loads 5 Kg of (a) Al-11.2% Fe (b) Al-11.2% Fe in Forged condition.

SEM images of the transverse section of the worn surface show that the buildup of oxide layer depends on sliding distance, composition, applied load and sliding velocity. In mild wear region after large sliding distance cracking and spalling of the oxide layer is observed in the wear track which turns into a deep groove after large sliding distance for all the Al-Fe composites. The highest percentage of oxide layer is formed at a lower amount of iron content as compared to the higher amount. XRD examination of wear debris shows the diffraction peaks corresponding to coexisting aluminum and alumina, different oxides of iron.

D . Friction studies

The variation of friction coefficient with sliding time is illustrated in Figure 19. This is a graphical representation of result obtained from the friction experiment at a 0.772 m/s sliding velocity and 5 Kg load. It is evident that the friction coefficient drastically decreases during the running in period. During the steady state period the friction coefficient is stabilizing. The average value of the friction coefficient at different normal loads is shown in Figure 20. The increase of the friction coefficient corresponds to the increase of the normal load. The increase rate is especially evident for load change from 15 to 50 N.

Figure 21 shows the dependence of the steady-state friction coefficient on the sliding speed, for various normal loads of 0 and 50N in dry sliding conditions. It can be found, in all the tested composite materials that the friction coefficient decreases with the increase of the sliding speed. The degree of change is especially prominent in the region of low speeds. Also, in all the tested composites, the friction coefficient increases with increase of the normal load.

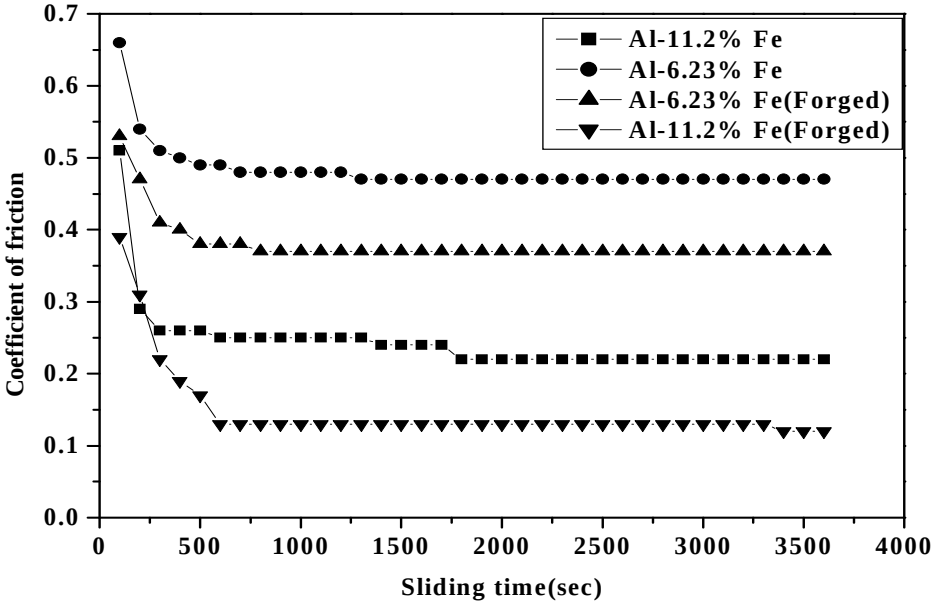

Fig19: Friction coefficient variation of Al-Fe composite during sliding time at fixed specific loads and sliding speeds.

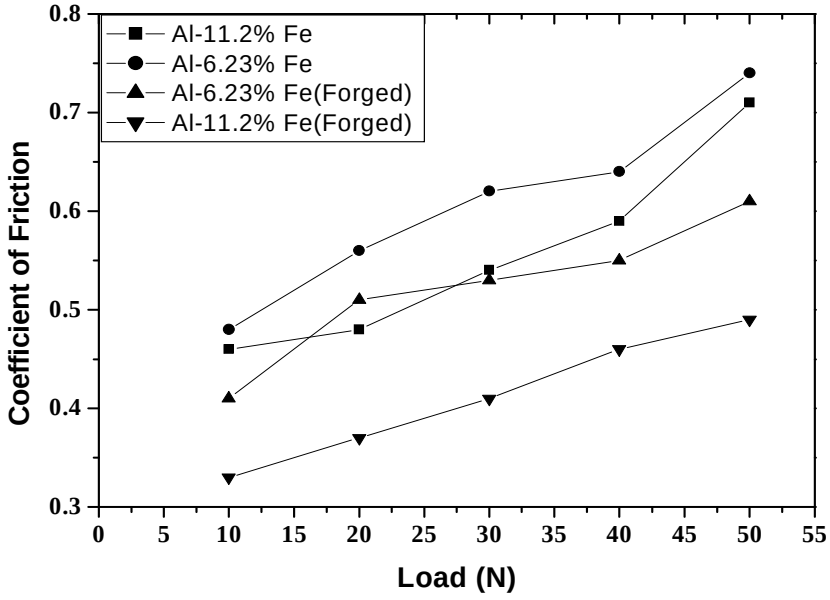

Fig 20: Coefficient of friction vs. applied load for Al-Fe composite

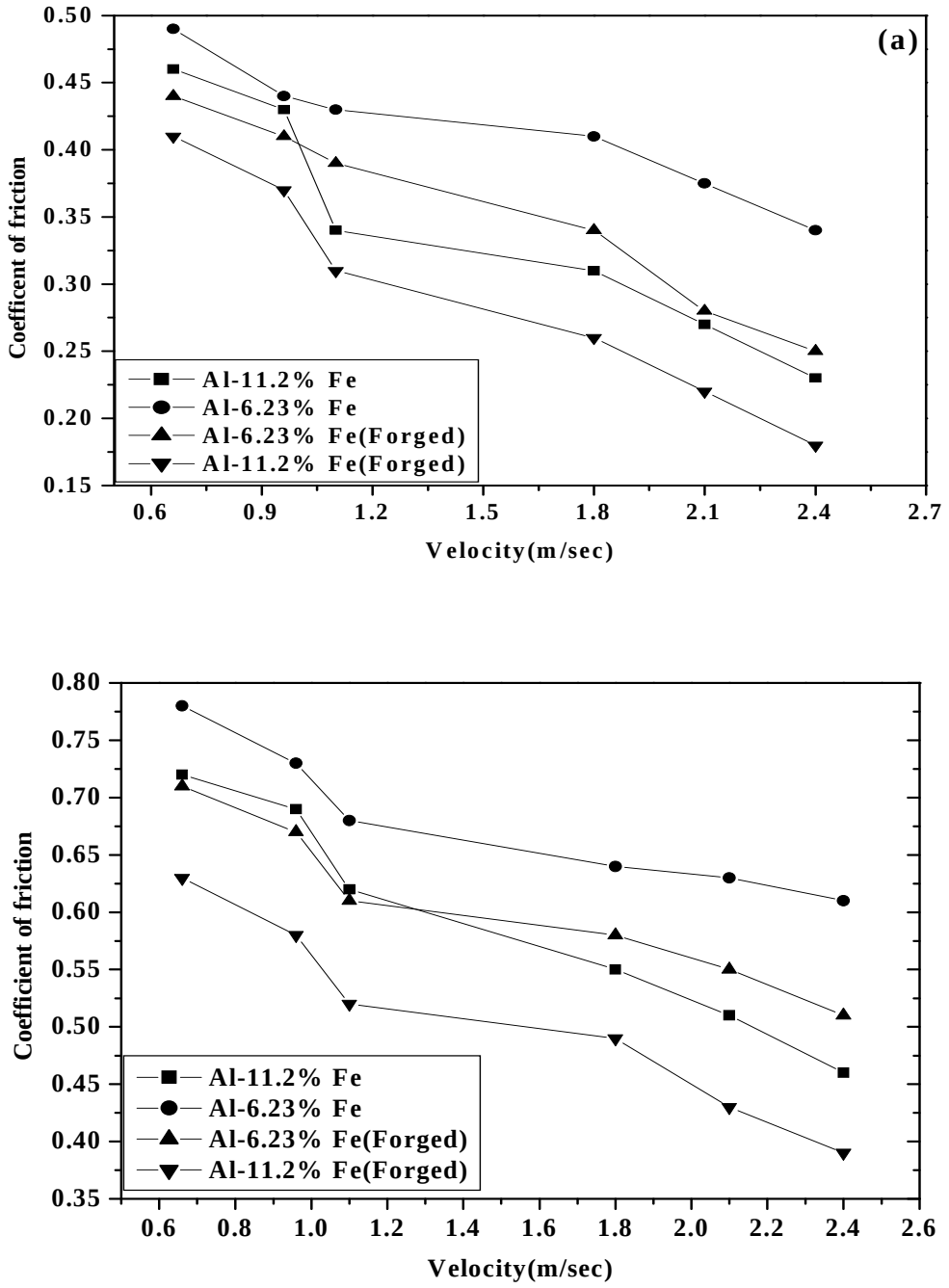

Fig20. Friction coefficient vs. sliding speed of Al-Fe composite at different applied loads: (a) 10N (b) 50N.

The worn surfaces of the samples from the SEM examination are shown in Figure 22 and 23. The worn surfaces of the cast Al-11.2 wt% Fe samples were noticed to be smoother than those of the forged Al-11.2%Fe samples, as shown Figure 23. Generally, the parallel ploughing grooves and scratches can be seen over all the surfaces in the direction of sliding. These grooves and

scratches resulted from the ploughing action of asperities on the counter disc of significantly higher hardness.

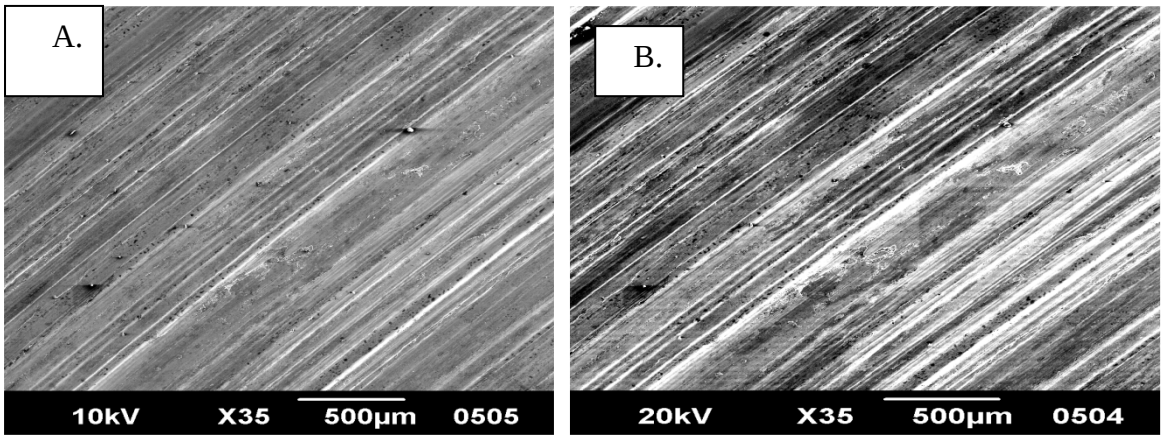

Fig 21. Wear surface of the Al-Fe composite in dry lubricated sliding condition for (a) 20N (b) 50 N of applied load and 0.26 m/s of sliding speed

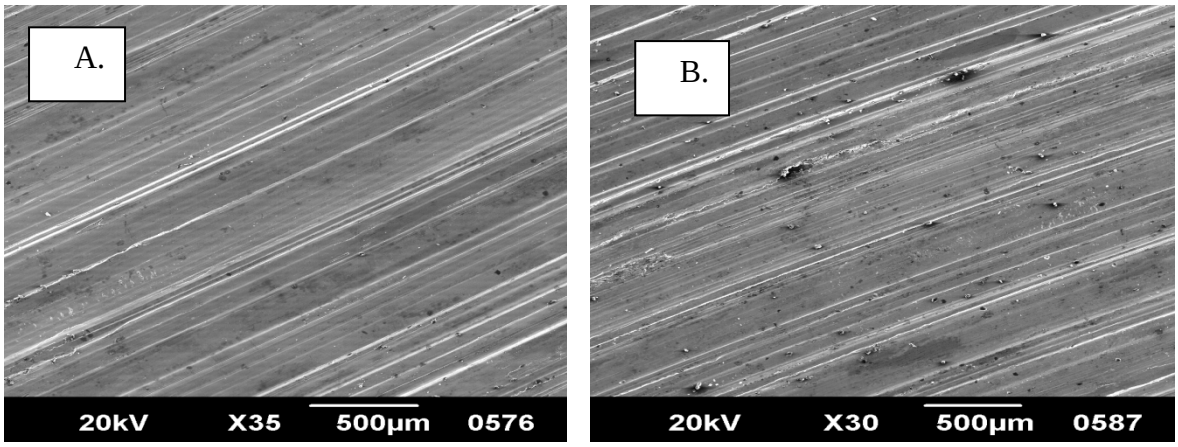

Fig 22. Wear surface of the forged Al-Fe composite in dry lubricated sliding condition for (a) 20N (b) 50 N of applied load and 0.26 m/s of sliding speed

It can be noticed from the Fig 19 that for all the contact loads, the friction coefficient of the forged Al-11.2%Fe composites is lowest among all the composites. The forged Al-11.2 % Fe shows the highest hardness, and from the metallographic observation $FeAl_3$ is uniformly distributed within the composite. The internetallics has higher hardness and also bear the larger load. The forged composite materials show the maximum hardness as compared to the as-cast composite. The wear rate is inversely proportional to the hardness of the materials. Forged Al-Fe composite shows minimum wear rate. Therefore it behaves like as lubricating materials in the machining components.

CONCLUSION

1. Iron can be successfully dispersed in aluminum melt by impeller mixing and bottom pouring chill casting technique.

2. Forged composite shows higher physical properties as compared to as-cast Al-Fe composite. Due to forging, harder phase like $FeAl_3$ is formed by forging the sample and then cooling immediately.
3. From the microstructure, harder phase i.e., $FeAl_3$ and its softer phase i.e.,$FeAl_6$,decomposed due to annealing at different temperature show a uniform distribution in the matrix
4. Al-Fe composites have superior mechanical properties like UTS, tensile strength, hardness along with superior ductility as compared to almost same compositions range of Al-Si alloys.
5. UTS, tensile strength, hardness of the composite decrease with increase the annealing temperature.
6 Feasibility study shows that like Al-Si alloys forged Al-Fe composites can make pistons.
7 Al-11.2%Fe in forged condition shows the minimum coefficient of friction and Al-6.23% Fe show the higher values.

REFERENCES

[1] D. J. Lloyd: Int. Mater. Rev. **(1994)**, vol. 39, pp. 1–23.
[2] P. Rohatgi: AFS Trans., **(2001)**, pp. 1–133.
[3] I.A. Ibrahim, F.A. Mohamed, and E.J. Lavernia: J. Mater. Sci.**(1991)**, vol. 26, pp. 1137–56.
[4] D.J. Lloyd: Int. Mater. Rev., **(1994)**, vol. 39 (1), pp. 1–23.
[5] S. Ray: J. Mater. Sci., **(1993)**, vol. 28, pp. 5397–5413.
[6] D.B. Miracle: Compos. Sci. Technol., **(2005)**, vol. 65, pp. 2526–40.
[7] R. Asthana: Adv. Perf. Mater. **(1998)**, vol. 5, pp. 213–55.
[8] N. Chawala and K.K. Chawala: J. Mater., **(2006)**, vol. 58 (11),pp. 67–70
[9] M. A. Chow., M. K. K , D. M. N , M.L. Ra. J. Mec. Mechat. Eng. , Bangladesh. **2011**;: 11 No: 01.
[10] M. Ramachandra and K. Radhakrishna "Students on Materials Science Engineering". Chennai, India. **2004**; 20- 22.
[11] Abbas, M.K. and Ibrahim, E.K., **2003**, Engineering and Technology Journal, University of Technology, Baghdad - Iraq, Vol. 22 (1), pp. 37-44.
[12]. Y T. Asmin, A. A. Khalid , M. M.Haque, Journal of Materials Processing Technology, **2004**, 153-154, p. 833-838.
[13]. S.A.Kori, Shekharaiah Chandra T.M., Wear, **2007**, 263, p. 745-75.
[14] S.M. Howard, R.L. Stephens, C.J. Newman, J.-Y.J. Hwang, A.M. Gokhale, T.T. Chen, T.P. Battle, M.L. Free, B.R. Davis, C.L. Harris, H. Henein, P.N. Anyalebechi, A.C. Powell, G.K. Krumdick, and C.K. Belt TMS (The Minerals, Metals & Materials Society), **2006**.
[15] K. Bouche´, F. Barbier and A. Coulet: Mater. Sci. Eng. A 249 (**1998**) 167–175.
[16]A. Bouayad, Ch. Gerometta, A. Belkebir and A. Ambari: Mater. Sci.Eng. A 363 (**2003**) 53–61
[17] T. Miyajima, Y. Iwai., Journal of Wear, Volume. 255, **2003**, pp 606- 616.